THE JOURNAL OF PHYSICAL CHEMISTRY B

Article

pubs.acs.org/JPCB

Energy Dependence of the Ruthenium(II)-Bipyridine Metal-to-Ligand-Charge-Transfer Excited State Radiative Lifetimes: Effects of $\pi\pi^*$(bipyridine) Mixing

Ryan A. Thomas,[‡] Chia Nung Tsai,[†] Shivnath Mazumder,[‡] I Chen Lu,[†] Richard L. Lord,[∥] H. Bernhard Schlegel,*[,‡] Yuan Jang Chen,*[,†] and John F. Endicott*[,‡]

[‡]Department of Chemistry, Wayne State University, Detroit, Michigan 48202, United States

[†]Department of Chemistry, Fu-Jen Catholic University, New Taipei City 24205, Taiwan, R.O.C.

[∥]Grand Valley State University, 1 Campus Drive, Allendale, Michigan 49401-9403, United States

Supporting Information

ABSTRACT: The variations in band shape with excited state energy found for the triplet metal to ligand charge transfer (^{3}MLCT) emission spectra of ruthenium-bipyridine (Ru-bpy) chromophores at 77 K have been postulated to arise from excited state/excited state configurational mixing. This issue is more critically examined through the determination of the excited state energy dependence of the radiative rate constants (k_{RAD}) for these emissions. Experimental values for k_{RAD} were determined relative to known literature references for Ru-bpy complexes. When the lowest energy excited states are metal centered, k_{RAD} can be anomalously small and such complexes have been identified using density functional theory (DFT) modeling. When such complexes are removed from the energy correlation, there is a strong ^{3}MLCT energy-dependent contribution to k_{RAD} in addition to the expected classical energy cubed factor for complexes with excited state energies greater than 10 000 cm^{-1}. This correlates with the DFT calculations which show significant excited state electronic delocalization between a π(bpy-orbital) and a half-filled dπ^*-(Ru^{III}-orbital) for Ru-bpy complexes with ^{3}MLCT excited state energies greater than about 16 000 cm^{-1}. Overall, this work implicates the "stealing" of emission bandshapes as well as intensity from the higher energy, strongly allowed bpy-centered singlet $\pi\pi^*$ excited state.

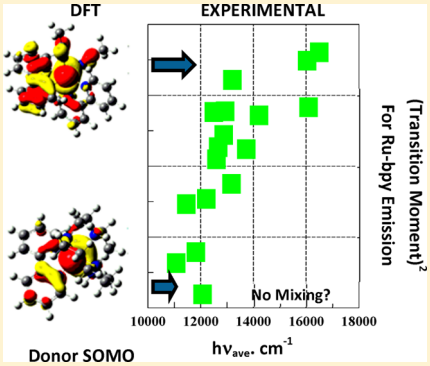

INTRODUCTION

Intramolecular excited state electron-transfer processes mediated by transition metal excited states are often key components of schemes for photocatalysis and solar energy conversion.[1−12] The effectiveness of transition metal complexes as mediators of the related photoprocesses is a function of the frontier orbitals occupied in the lowest energy excited states, the structural and energy differences of these electronic states from their respective ground states and their lifetimes. In dealing with these properties of electronic excited states of a donor (D)/acceptor (A) system, it is simplest to initially assume that D and A are electronically isolated in the ground state and in the charge transfer excited state:

$$\{D, A\} + h\nu \rightarrow \{D^+, A^-\}^* \quad (1)$$

When the D/A mixing is very small, the excited state properties can be treated in terms of small deviations from the properties of the isolated D^+ and A^- species.[13−18] However, our recent work combining spectroscopic studies with density functional theory (DFT) modeling has found several excited state properties of ruthenium-(D)/polypyridyl ligand-(A) complex excited states that differ from expectation based on simple limiting models.[19−24] Thus, when the donor and acceptor are covalently linked, and since the energy differences between excited states are often not large in heavy metal complexes, theoretical models based on such weak coupling limits can be misleading.[25] In the present paper we examine the 77 K radiative properties (spectra, quantum yields, and lifetimes) of simple Ru-bpy complexes in order to gain more critical insight into the effects of electronic mixing on metal to ligand charge transfer (MLCT) excited state properties. To this end we have examined the energy dependence of the radiative rate constants and of DFT-calculated parameters for evidence of excited state/excited state mixing.

The excited state lifetime depends on the rate constants for the available relaxation pathways and can be represented as

$$\tau_{em} = (\sum_n k_n)^{-1} = (k_{obsd})^{-1} \quad (2)$$

The most important relaxation pathways are usually[26] (1) intersystem crossing between excited states of different spin multiplicity, k_{ISC}; (2) internal conversion between excited states

Special Issue: John R. Miller and Marshall D. Newton Festschrift

Received: October 31, 2014
Revised: March 9, 2015
Published: March 12, 2015

DOI: 10.1021/jp510949x
J. Phys. Chem. B 2015, 119, 7393−7406

of the same spin multiplicity, k_{IC}; (3) nonradiative pathways, k_{NRD}, that depend on the rates of transfer of excited state energy to ground state vibrational modes;[26,27] and (4) the radiative relaxation pathway, k_{RAD}. The rate of radiative relaxation determines the maximum possible excited state lifetime since, if all other relaxation pathways are blocked (k_n = 0 for all $n \neq$ RAD), the excited state will relax only by means of an emission characteristic of the chromophore. It is usually assumed that the emitting state is the lowest energy excited state ("Kasha's Rule")[28] so that k_{IC} and k_{ISC} are relatively unimportant and that $\tau_{em}^{-1} \approx k_{RAD} + k_{NRD}$. However, there are now several examples of Ru-bpy complexes with strong phosphorescent emissions from MLCT excited states that are not the lowest energy excited states,[21,29,30] in violation of Kasha's rule,[28] and this can complicate the interpretation of τ_{em} and k_{RAD}.[23] In general, the value of k_{NRD} should decrease as the excited state energy increases, while that of k_{RAD} is expected to increase so that the radiative rate constant can become a major factor in determining the lifetimes of high energy photosensitizers.[26]

Many ruthenium-bipyridine, Ru-bpy, chromophores have been prepared and characterized,[5,31] and some of these complexes provide a range of useful model systems for this study. The emitting state of these ruthenium complexes is a triplet metal to ligand, ^{3}MLCT, excited state, and the emission to the singlet ground state, S_0, involves a change of spin multiplicity. The formalisms used for k_{RAD} in most discussions are based on an expression of Einstein's for atomic fluorescence spectra:[26,32]

$$k_{RAD} = C_r \nu^3 \eta^3 M^2 \tag{3}$$

$|\vec{M}|$ is the transition dipole moment, ν is the transition frequency (corresponding to an emission energy $h\nu$), η is the refractive index, $C_r = (16\pi^3)/(3\varepsilon_o c^3 h)$, and ε_o is the vacuum permittivity. However, the phosphorescence emission of molecular excited states requires additional considerations. Important among these is how best to treat $|\vec{M}|$. The transition dipole moment can be partitioned into the contributions of an electronic contribution, $M_{el(DA)}$, and a Franck–Condon factor (FC), which accounts for the emission contributions of the excited state vibronic distortions, $|\vec{M}| = |\vec{M}|_{el}(FC)$. In some limits of weak electronic coupling between the excited state and the ground state in a two state donor/acceptor complex (D/A), it is possible to represent $|\vec{M}|_{el}$ by[17,18,24,33]

$$\vec{M}_{el(DA)} \approx \frac{H_{DA}}{\nu_{DA}} \overrightarrow{\Delta\mu_{DA}} \tag{4}$$

where H_{DA} is the electronic matrix element for mixing the ground state (DA) and excited state (D^+A^-) electronic configurations, ν_{DA} is the (DA) → (D^+A^-) transition frequency and $\Delta\mu_{DA}$ is the difference in ground state and excited state molecular dipole moments. Equation 4 would have the effect of reducing the excited state energy dependence of k_{RAD} to first order from the third order dependence in eq 3, but it is not likely that it could be applicable to a spin forbidden transition. While spin–orbit coupling is likely to be important in promoting such transitions in heavy metal complexes, it will be most important when the spin–orbit coupled electronic state is near in energy to the emitting state and therefore a higher energy excited state.[34,35]

The various formulations of the transition moment summarized above assume that no complications arise due to the mixing of different electronic excited states. However, a notable exception to this assumption has been discussed by Mulliken and Person[17] and by Bixon et al.[36] When a local transition (i.e., donor or acceptor centered) is very strongly allowed and sufficiently near in energy to the donor–acceptor charge transfer (DACT) excited state it can significantly alter the values of $|\vec{M}|$. Thus, based on the configurational mixing of two excited states,

$$\vec{M} \approx (\overrightarrow{M_{D^+A^-}} + \alpha_{CT,IL} \overrightarrow{M_{IL}})N \tag{5}$$

where N is the normalizing constant, $\overrightarrow{M_{D^+A^-}}$ is the transition dipole moment for a "pure" (diabatic) DACT transition, $\alpha_{CT,IL} \approx (H_{CT,IL})/(\Delta E_{CT,IL})$, $H_{CT,IL}$ is the matrix element for the mixing of the excited states, $\Delta E_{CT,IL}$ is the vertical energy difference between the charge transfer (CT) and internal ligand (IL) excited states, and $\overrightarrow{M_{IL}}$ is the transition dipole moment for a "pure" (diabatic) local transition.[17] The vector notation is used here because the two transition dipole moments are not necessarily collinear.

Several other factors need to be considered in assessing the transition dipole moments for phosphorescence in complexes containing the Ru-bpy chromophore: (a) The difference in spin multiplicity of the (DA) and (D^+A^-) states requires a multiplicity factor, and this contributes to the forbiddeness of the transition. (b) There are typically molecular distortions in a number of vibrational modes, and these couple to the electronic transition (see Figure 1) as is evident from the vibronic sideband features of the emission spectra.[37] The measured values of k_{RAD} correspond to the composite of the different k_{RAD}(vib) values contributed by the vibronic transitions at $E_{max(vib)}$. This requires the use of a spectrally weighted average energy which can be approximated[26] and is discussed below. (c) An appreciable excited state nuclear displacement requires that the ^{3}MLCT excited state potential energy (PE) minimum has different nuclear coordinates than those of the S_0 PE minimum. Consequently, a vertical transition from the excited state minimum will intersect the ground state surface at some

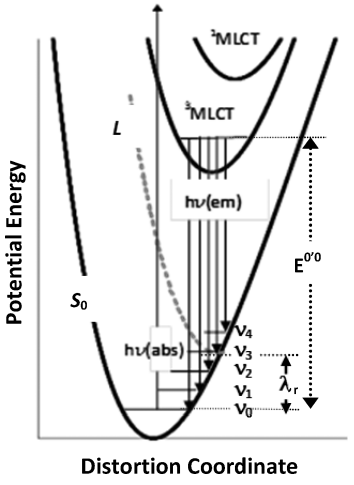

Figure 1. Qualitative PE curves illustrating features of the emission from a charge transfer excited state which is distorted in several vibrational modes, ν_n (n = 0, 1, 2, etc.). The dashed curve, L, illustrates the limit in which $E^{0'0} = \lambda_r$.

DOI: 10.1021/jp510949x
J. Phys. Chem. B 2015, 119, 7393–7406

energy (the reorganizational energy) $\lambda_r > 0$. These issues are discussed further below.

The work reported here is a result of our attempts to understand the origin and implications of the excited state energy dependence of the vibronic sideband amplitudes that are found in the emission spectra of Ru-bpy chromophores.[37−39] Computational modeling has indicated that the wide range of implicated excited state distortions found for these systems originates from the electronic mixing of the Ru-centered orbitals of the Ru/bpy ^{3}MLCT excited state with the bpy ligand π and π^* orbitals, or alternatively from the electronic mixing between the ^{3}MLCT (or the $\{D^+,A^-\}$) and $\pi\pi^*$ excited states.[20] The radiative rate constants obtained in this study are more consistent with eq 5 than with either eqs 3 or 4. Similar inferences have been reported for some bridged electron transfer systems with organic donors and acceptors.[36]

EXPERIMENTAL SECTION

1. Materials and Synthesis of Compounds. Pyrazine (pz), Pyridine (py), 4-acetyl-pyridine (acpy), 2,2′-bipyridine (bpy), ethylenediammine (en), and ferrocene and trifluoromethanesulfonic acid (HOTF) were purchased from Aldrich; $[Ru(NH_3)_6]Cl_3$ and NH_4PF_6 were purchased from STREM Chemicals. These materials were used without further purification. The syntheses of tris(1-pyrazolyl)methane (tpm),[40,41] $[Ru(bpy)_2(acac)](PF_6)$,[39,42] $[Ru(bpy)_2(NCCH_3)_2](PF_6)_2$,[39] $[Ru(bpy)_2(ox)]$,[39] $[Ru(NH_3)_5Cl]Cl_2$, $[Ru(NH_3)_5(H_2O)](PF_6)_2$, *cis*-$[Ru(NH_3)_4(Cl)_2]Cl$ and *mer*-$[Ru(NH_3)_3(bpy)(H_2O)](PF_6)_2$[43] have been reported previously. Variations in previously reported syntheses were used for the following compounds: $[Ru([9]aneS_3)(bpy)(CN)](PF_6)$,[44] *mer*-$[Ru(NH_3)_3(bpy)(py)](PF_6)_2$,[23] *mer*-$[Ru(NH_3)_3(bpy)(pz)](PF_6)_2$,[23,45] $[Ru(bpy)_2(en)](PF_6)_2$,[46] $[Ru(bpy)_2(CN)_2]$,[47,48] $[Ru(bpy)([14]aneN_4)](PF_6)_2$,[38] $[Ru(bpy)(NH_3)_4](PF_6)_2$,[49] and $[Ru(bpy)(tpm)(NCCH_3)](PF_6)_2$.[50]

mer-[Ru(NH$_3$)$_3$(bpy)(L)](PF$_6$)$_2$, L = acpy and CH$_3$CN. A sample of 200 mg of *trans*-$[Ru(NH_3)_3(bpy)(H_2O)](PF_6)_2$ and a 3 molar excess of ligand (acpy or AN) were added to 10 mL of a degassed acetone solution under argon, and the mixture was stirred for 3 h. Then, the red reaction mixture was filtered, and 2 mL of saturated NH_4PF_6 aqueous solution was added; the solution volume was then reduced to 3 mL in an ice bath, and the resulting red product was removed by filtration. The product was washed with 1 mL of cold water followed by a second wash with 5 mL of cold ether. The product was dried in an oven under vacuum. For *mer*-$[Ru(NH_3)_3(bpy)(acpy)](PF_6)_2$, anal. calcd for $C_{17}H_{24}N_6OP_2F_{12}Ru_1$: C, 28.38; N, 11.68; H, 3.36. Found: C, 28.51; N, 11.64; H, 3.20. ^{1}H NMR (acetone-d_6): δ 2.53 (br, 6H), 2.72 (s, 3H), 3.54 (br, 3H), 7.53 (t, 1H), 7.70 (t, 1H), 7.96−8.11 (m, 4H), 8.57−8.69 (m, 3H), 9.20 (d, 2H), 9.35 (d, 1H). ^{13}C NMR (acetone-d_6): δ27.02, δ123.70, δ123.90, δ123.97, δ126.54, δ126.56, δ135.73, δ136.98, δ142.71, δ142.72, δ154.73, δ157.90, δ160.98, δ161.41, δ197.61. For *mer*-$[Ru(NH_3)_3(bpy)(AN)](PF_6)_2$, anal. calcd for $C_{12}H_{20}N_6P_2F_{12}Ru_1$: C, 22.54; N, 13.15; H, 3.15. Found: C, 22.78; N, 13.01; H, 3.02. ^{1}H NMR (acetone-d_6): δ 2.32 (br, 6H), 2.73 (s, 3H), 3.40 (br, 3H), 7.55 (t, 1H), 7.62 (t, 1H), 7.95 (t, 1H), 8.03 (t, 1H), 8.48−8.54 (m, 2H), 9.24 (d, 1H), 9.45 (d, 1H). ^{13}C NMR (acetone-d_6): δ4.42, δ123.53, δ123.62, δ126.40, δ126.58, δ128.45, δ135.67, δ136.70, δ154.34, δ155.57, δ160.80, δ161.23.

2. Instrumentation. The electrochemical measurements were performed using an Epsilon Electrochemical Workstation. Cyclic voltammograms (CVs) and differential pulse voltammograms (DPVs) were obtained in acetonitrile solution, which contained 10^{-3} M complex and 0.1 M *n*-tetrabutylammonium hexafluorophosphate (*n*-TBAH) at scan rates of 100 mV/s and 4 mV/s, respectively. A three-electrode system consisting of a Pt-disk (1 mm) as a working electrode, polished with 0.1−0.3 μm Baikowski alumina suspension, a Pt-wire as the counter electrode, and Ag/AgCl as the reference electrode was used. Ferrocene (0.437 V vs Ag/AgCl in acetonitrile) was used as the internal standard.

The 298 K absorption spectra in the solution of CH_3CN were determined with a Shimadzu UV-2101PC or UV-3101PC spectrophotometer. Absorption spectra in 90 K butyronitrile and alcohol (v/v' = 4/1 of ethanol/methanol) glasses were obstained as described in detail elsewhere[21,23] using a calibrated Xe emission lines for wavelength and an Oriel model 63966 Quartz Tungsten Halogen (QTH) lamp for intensity. The calibration provided with the QTH lamp was in power units and was converted to units of photonic amplitude. A QTH lamp was also used as the light source in spectroscopic and yield measurements. The low-temperature absorption spectra were collected using either

(a) An Oxford Instruments OptistatCF Static Exchange Gas Continuous Flow Cryostat with liquid nitrogen as the cryogen was used at 90 K with NSG Precision Cells, Inc. cryogenic square 1 cm quartz cuvettes with an ANDOR Shamrock 500 spectrometer with dual exit ports and equipped with three gratings: 150 l/mm, 800 nm blaze; 600 l/mm, 500 nm blaze; and 300 l/mm, 1200 nm. ANDOR Newton DU920-BV (for the visible range) and ANDOR iDus-InGaAs DU490A-1.7 (for the NIR) detector heads were mounted on the exit ports of the Shamrock 500 spectrometer. Light was collected with a lens and guided to an ANDOR SR500i F#-matcher by a Thorlabs 3 mm Core Liquid Light Guide LLG0338-4 (wavelength range 340−800 nm).

(b) A P/N 21530 Specac variable temperature cell (−190 °C ∼ 250 °C) as the controlled-temperature cell holder with liquid or glass samples in a square 1 cm quartz cuvette. The detection system contained a motor-driven Jobin Yvon H-10 Vis monochromator, a Hamamatsu R928 phototube with a Jobin-Yvon (JY) PMT-HVPS power supply, a JY Spectracq2 for data acquisition, and the JY SynerJY software for data acquisition and data analysis.

Details for obtaining emission spectra in 77 K glasses are described in detail elsewhere.[20,51,52] The emission spectra were collected using slightly different systems:

(a) An ANDOR Shamrock 500 spectrometer with equipped with three gratings with an ANDOR Newton DU920-BV (for the visible range) and ANDOR iDus-InGaAs DU490A-1.7 (for the NIR) detector heads were mounted on the dual exit ports. Light was collected with a lens and transmitted by means of Oriel 3 mm Core Liquid Light Guide 77634 (wavelength range 420−2000 nm).

(b) A HORIBA JOBIN YVON iHR 550 spectrometer with three gratings (300 l/mm, 600 nm blaze; 300 l/mm, 1 μm blaze; and 600 l/mm, 1 μm blaze) and a HORIBA Symphony InGaAs-1700 (for the NIR) detector head were mounted on the exit port. This system was operated using the SynerJY software. The detector heads were

DOI: 10.1021/jp510949x
J. Phys. Chem. B 2015, 119, 7393−7406

cooled to −90 °C and the spectrometers were purged with dry N_2.

The 77 K emission lifetimes were determined using Spectra Physics VSL-337ND-S nitrogen laser-pumped DUO-210 Dye laser system, Hamamatsu P9220 PMT/E717−63 mounted on a Jobin-Yvon H-100 spectrometer and National Instruments NI PCI-5154, 2 GS/s, 1 GHz Digitizer w/8 MB/ch onboard memory PC card as described previously.[21] Emission yields in 77 K glasses were obtained as described in detail elsewhere.[21,23]

3. Some General Considerations and Aspects of the Data Analysis. The experimental emission intensity, I_{em}, is proportional to the emission quantum yield, ϕ_{em}, and for a chromophore that emits from the lowest energy excited state with γ the efficiency of forming the emitting state,

$$\phi_{em} = \gamma \frac{k_{RAD}}{k_{RAD} + k_{NRD}} \tag{6}$$

There are reasons to suspect that $\gamma < 1$ for some Ru^{II} complexes that emit strongly even though they have lower energy metal centered excited states.[21,23] For complexes that the DFT modeling indicates that a ^{3}MLCT excited state is the lowest energy triplet state, we have assumed that $\gamma = 1$ for reasons discussed below.

In molecules, eq 3 should apply to each coupled vibrational state and each of these vibronic transitions, $\nu_0' \rightarrow \nu_0$, $\nu_0' \rightarrow \nu_1$, $\nu_0' \rightarrow \nu_2$, etc., will have different values of ν_{em}, $|\vec{M}|$ and contribute to the total (or integrated) emission intensity and k_{RAD}.[26] The observed mean rate constant is the weighted average of the individual vibronic component contributions, $k_{RAD(n)}$. For n vibronic component contributions to the emission spectrum with very small bandwidths (full width at half height <50 cm^{-1}) so that there is no overlapping of their intensity contributions, then

$$k_{RAD(ave)} = \frac{\sum_{n=0}^{all} (FC)_n k_{RAD(n)}}{\sum_{n=0}^{all} (FC)_n} \tag{7}$$

or, based on eq 3,

$$k_{RAD(ave)} \approx \frac{C_r \eta^3 \sum_{n=0}^{all} (FC)_n^2 \nu_n^3 |\overrightarrow{M_n}|^2}{\sum_{n=0}^{all} (FC)_n^2} \tag{8}$$

Since the component band widths in the observed spectra are typically hundreds of wave numbers at 77 K, there is appreciable overlapping of vibronic intensity contributions and the effective value of $k_{RAD(m)}$ at any observed emission energy, $h\nu_m$, is in principle a sum over all the vibronic intensity contributions of each vibrational mode, ν_i, weighted by its amplitude, A_i, at $h\nu_m$. In principle, the weights for the $k_{RAD(m)}$ contributions might be represented in terms of Franck−Condon factors for the contributing vibrational modes. However, the excited states of this class of complexes have distortions in more than 10 fundamental vibrational modes in the range of 100−1700 cm^{-1},[20,53,54] which leads to a large number of higher order contributions from harmonics and combination bands to the observed emission spectra.[20,37−39] Consequently the $(FC)_m$ parameters are very hard to evaluate (see eq 10). Birks has suggested a more practical approach to treating molecular emission spectra for this limit,[26] by representing k_{RAD} as a function of $\nu_{(ave)}$, (the subscript "m" designates the frequency (in wavenumbers when energy is involved) of the measurement),

$$\nu_{ave} \approx \frac{\int \nu_m I_m \, d\nu_m}{\int I_m \, d\nu_m} \tag{9}$$

We have used such values of $h\nu_{ave}$ in our analysis of the energy dependency of the Ru-bpy radiative lifetimes.

The emission band shape and vibronic side bands can be interpreted in terms of a Franck−Condon analysis, and some relatively simple details are presented here to clarify aspects of the discussion below. When the ground (g) and excited (e) state differ in geometry only in the coordinates of the kth normal mode of the ground state and assuming Gaussian component bandshapes, the emission spectrum can be represented as[24,27,39,55−57]

$$(I_{\nu_m})_k = I_{\nu_m(0'0)} + C\left(\sum_{j=1}^{\infty} (FC)_{j,k}^2\right) \tag{10}$$

$$C = \frac{64\pi^4}{3h^3c^3 \ln 10} \frac{\nu_m{}^3 \eta^3 M_{eg}^2}{(4\pi\lambda_s k_B T)^{1/2}} \tag{11}$$

$$F_{j,k} = \frac{S_k{}^j e^{-S_k}}{j!}$$

$$S_k = \frac{\lambda_k}{h\nu_k} \tag{12}$$

$$g_{j,k} = E_{eg}^{0'0} - \lambda_s - jh\nu_k - h\nu_m \tag{13}$$

$$I_{\nu_m(0,0)} \cong C e^{\{-[E_{eg}^{0'0} - h\nu_m]^2/(\Delta\nu_{1/2}{}^2/4 \ln 2)\}} \tag{14}$$

$$(FC)_{j,k}^2 = F_{j,k} e^{-\{4g_{j,k}^2 \ln 2/\Delta\nu_{1/2}^2\}} \tag{15}$$

The first term in eq 10 corresponds to the transition between the PE minima of the two states, {e,0′} → {g,0}, and can be represented as the spectral intensity of the band origin with a full width at half height $\Delta\nu_{1/2}$.[37,39]

The second term in eq 10 is the sum over the amplitudes of the single vibrational mode k, and it includes the fundamental (or first order) and harmonic vibrational contributions. In these equations, η is the index of refraction, ν_m is the frequency of the incident radiation, M_{eg} is the electronic part of the transition dipole, λ_s is the solvent reorganizational energy and other very low energy displacement modes (frequencies $\nu_s < \approx 2k_BT$), and c is the speed of light.

Distortions in a large number (>10) of different vibrational modes typically contribute to the emission bandshapes[53,54,58,59] and these contributions are not generally resolved in the 77 K emission spectra, so the emission spectrum must be represented as the sum of the band origin (0′0), all the progressions in single vibrational modes (k) and all the vibronic combination bands,

$$I_{\nu_m} = I_{\nu_m(0,0)} + \sum_{k=1}^{all} \sum_{j=1}^{\infty} (I_{\nu_m})_{j,k} + \sum_{p=1}^{all} \sum_{k=1}^{all \neq p} \sum_{i=1}^{\infty} \sum_{j=1}^{\infty} (I_{\nu_m})_{i,j,k,p} + \ldots \tag{16}$$

where the third term on the right contains contributions of the combination bands formed from two different fundamental vibrational modes (k and p), with

DOI: 10.1021/jp510949x
J. Phys. Chem. B 2015, 119, 7393−7406

$$F_{i,j,k,p} = \frac{S_k^i S_p^j e^{-(S_k+S_p)/2}}{(j+i)!} \quad (17)$$

Equations 10−15 can be combined with resonance-Raman parameters to calculate the vibronic bandshapes of emission spectra or, in combination with those parameters, used as a basis for fitting observed spectra.[37−39] The DFT calculations of emission bandshapes use somewhat different procedures for the calculations, but have the same general features.[60−64]

We used $[Ru(bpy)_3]^{2+}$, $[Os(bpy)_3]^{2+}$, and/or $[Ru(bpy)_2(en)]^{2+}$ in 77 K ethanol/methanol glasses as references for the determination of emission quantum yields. The quantum yields reported for these complexes, $\Phi_r \approx 0.38$, 0.038,[65,66] and 0.022,[66] respectively, (λ_{max} = 435.8 nm excitation), were used as references for the determination of relative quantum yields for the complexes studied. Equation 18 was used to calculate the relative quantum yield of target complex (Φ_{tc})[66,67]

$$\frac{\Phi_{tc}}{\Phi_r} = \frac{\eta_{tc}^2 I_{tc}}{\eta_r^2 I_r} \times \frac{1-10^{-A_r}}{1-10^{-A_{tc}}} \approx \frac{I_{tc}A_r}{I_r A_{tc}} \quad (18)$$

where I_{tc} and I_r are the integrated areas under the emission spectra of target complex (tc) and reference (r), respectively, A_{tc} and A_r are the absorbance of interest, respectively, η is the refractive index of the solvent, and $(\eta_{tc}^2/\eta_r^2) = 1$ for the reference and sample in the same solvent system. We used cylindrical 2 mm i.d. fluorescence cells immersed in a Dewar with liquid nitrogen for the 77 K emission yield determinations. The sample path length for the absorbance in eq 18 is not well-defined for these cells, but the effective pathlengths did not vary much since the cell geometry and position were the same for sample and reference solutions. Solute concentrations were in the 0.01−1 mM range in order to achieve absorbances of about 1 in 1 cm; however, in the 2 mm i.d. cylindrical cells, this amounts to an average absorbance of much less than 0.2 in the sample solutions, and the relatively higher solute concentrations were used for weakly absorbing and/or very weakly emitting substrates. Solutions that showed signs of inhomogenieties (light scattering, broadened and anomalous spectra, and/or multicomponent and irreproducible decay behavior) were discarded.

4. Computational Procedures. Electronic structure calculations were carried out using DFT[68] as implemented in the development version of Gaussian,[69] with B3PW91 functional[70−72] and SDD basis set and pseudopotential[73] on the metal, and 6-31G(d) basis[74,75] on the lighter atoms. Wave functions were tested for SCF stability,[76−78] and all of the optimized structures were confirmed as minima by analyzing the harmonic vibrational frequencies. The ground state singlet and triplet states were computed using the standard SCF method, and analytical frequencies were obtained for each. Solvation effects (in acetonitrile) were accounted for using the implicit SMD continuum solvation model[79] and were included during structure optimization. The isodensity plots of the orbitals were visualized using GaussView.[80] Our previous studies[20] have found that variation of the nuclear charge on Ru (Z_{Ru}) can mimic the effect of changing the ancillary ligands for a number of Ru(bpy) complexes, and changing Z_{Ru} from 43.5 to 44.5 allowed us to probe the emission energies covering the range observed experimentally. The variations in the 77 K emission spectral band shapes were at least semiquantitatively reproduced for those complexes using the Franck−Condon approximation as implemented in Gaussian by Barone et al.[60−64] In our previous work,[20] vibrationally resolved emission spectra were computed using the calculated intensity values instead of the Franck−Condon amplitudes. In the present work, Franck−Condon amplitudes have been used to calculate the first-order vibronic sideband contributions (Figure 3) of the $[Ru(NH_3)_4bpy]^{2+}$-like complexes. The intensities calculated by the Gaussian program are in the form of energy resulting in a $(\nu_{em})^4$ factor multiplying the Franck−Condon contribution.[64] The spin−orbit coupling is not included in the calculations, and it is assumed that the emission is fully allowed with the electric transition dipole moment arbitrarily set to 1 au.[64]

RESULTS

A. 77 K Emission Spectra, Lifetimes, and Quantum Yields. We have determined or redetermined the 77 K emission spectra, lifetimes, and quantum yields of several complexes in two different solvents. The normalized spectra in 4:1 ethanol:methanol glasses are shown in Figure 2, and the spectroscopic observations are summarized in Table 1 and Supporting Information Table S2.[81] As has been previously discussed, the amplitude of the dominant vibronic sideband decreases markedly as the excited state energy decreases.[20,37−39]

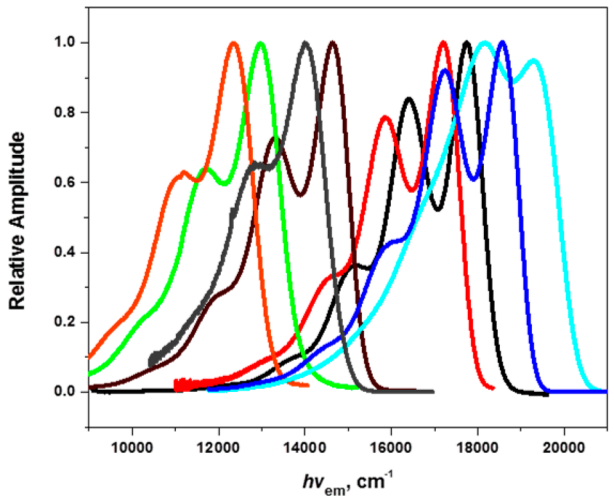

Figure 2. 77 K emission spectra of the complexes. From right to left: $[Ru(bpy)([9]aneS_3)(CN)]^+$ (cyan); $[Ru(bpy)_2(NCCH_3)_2]^{2+}$ (blue); $[Ru(tpm)(bpy)(NCCH_3)]^{2+}$ (black); $[Ru(bpy)_3]^{2+}$ (red); $[Ru(bpy)_2(NH_3)_2]^{2+}$ (violet); $[Ru(bpy)_2(acac)]^+$ (gray); $[Ru(bpy)(en)_2]^{2+}$ (green); $[Ru(bpy)(NH_3)_4]^{2+}$ (orange).

B. Computational Results. *1. Some Implications of Previous DFT Modeling of ^{3}MLCT Excited States.* The vibronic bandshapes, which were previously calculated using the Franck−Condon approximation as implemented in Gaussian[69] by varying the charge of the Ru-center while holding the ancillary ligands constant, change dramatically with excited ^{3}MLCT excited state energy.[20] The gray curves in Figure 3 are the calculated vibronic amplitudes of the vibrational fundamentals $\sum_{k=1}^{all}(FC)_{l,k}^2$ (see eqs 10−13), based on the reported $[Ru(NH_3)_4bpy]^{2+}$ resonance-Raman parameters[53] (Table 2), with $E_{eg}^{0,0}$ energies equal to those used by Lord et al.,[20] and illustrate that in the absence of configurational mixing, there is no variation of band shape with excited state energy. By contrast, the DFT-calculated single mode progressions, as in $\sum_{k=1}^{all}\sum_{j=1}^{\infty}(FC)_{j,k}^2$ (see eqs 10 and 15), at these energies illustrate

DOI: 10.1021/jp510949x
J. Phys. Chem. B 2015, 119, 7393−7406

Table 1. 77 K Emission Rate Constants and Quantum Yields of the Complexes[a]

code	$(L)_4$ for $[Ru(L)_4bpy]^{m+}$ complexes	$h\nu_{max}$(em), $cm^{-1}/10^3$ bun {alc}	$h\nu_{ave}$, $cm^{-1}/10^3$ bun {alc}	k_{obs}, μs^{-1}[b] bun {alc}	$\phi \times 10^4$[c] bun {alc}	k_{RAD}, μs^{-1}[d] bun {alc}	k_{NRD}, μs^{-1}[e] bun {alc}
1	([9]aneS$_3$)(CN)	{19.2}	{17.5}	{0.063}	{3600 ± 1100}	{0.023 ± 0.007}	{0.040 ± 0.007}
2	(bpy)(CH$_3$CN)$_2$	{18.5}	{16.8}	{0.120}	{6300 ± 1400}	{0.076 ± 0.016}	{0.044 ± 0.016}
3	(tpm)(CH$_3$CN)	17.74	16.50	0.15	5400 ± 800	0.081 ± 0.012	0.069 ± 0.012
4	(bpy)$_2$	17.25[f] {17.12}[g]	16.09 {16.04}	0.13[f] {0.19}[g]	4500 ± 700 {3800}[g]	0.059 ± 0.009 {0.072}[g]	0.072 ± 0.009, {0.12}[g]
5	(bpy) (CN)$_2$	{17.12}[g]	{15.87}	{0.25}[g]	{2700}[g]	{0.068}[g]	{0.19}[g]
6	(bpy)(en)	15.11;[f] {14.78}[g]	14.21 {13.95}	0.69[f] {1.0}[g]	570 ± 80; {0.022}[g]	0.039 ± 0.006; {0.023}[g]	0.65; {1.0}[g]
7	(bpy)(NH$_3$)$_2$	14.70;[f] {14.40}	13.73 {13.48}	1.7[f] {2.9}	180 ± 40; {37 ± 7}	0.031 ± 0.006; {0.011 ± 0.002}	1.7; {2.9}
8	(bpy)(ox)	{14.2}[g]	{12.9}	{1.8}[g]	{130}[g]	{0.024}[g]	{1.8}[g]
9	(bpy)(acac)	{13.9}	{12.9}	{1.4}	{230 ± 40}	{0.032 ± 0.006}	{1.4}
10	(NH$_3$)$_3$(pz)	13.98[h] {13.78}	13.20 {12.91}	4.8[h] {8.7}	85 ± 17; {26 ± 6}	0.041 ± 0.008 {0.023 ± 0.005}	4.7 {8.7}
11	(NH$_3$)$_3$(CH$_3$CN)	13.81 {13.57}	12.92 {12.66}	4.6 ; {8.6}	55 ± 10; {29 ± 6}	0.025 ± 0.005 {0.025 ± 0.004}	4.5 ; {8.6}
12	(NH$_3$)$_3$(acpy)	13.78 {13.32}	12.93 {12.50}	5.9 ; {12}	56 ± 17; {25 ± 5}	0.033 ± 0.010 {0.029 ± 0.006}	5.9 ; {12}
13	(NH$_3$)$_3$(py)	13.48[h] {13.11}	12.60 {12.21}	6.3;[h] {12}	36 ± 7; {13 ± 3}	0.023 ± 0.004 {0.016 ± 0.003}	6.2 {12}
14	([14]aneN$_4$)	13.99;[f] {13.84}	13.13 {13.04}	0.98;[f] {1.8}	86 ± 12 {26 ± 4}	0.0084 ± 0.0012 {0.0046 ± 0.0008}	0.97 {1.8}
15	(en)$_2$	13.01;[f] {12.70}	12.07 {11.82}	9.5[f] {19 ± 1}	20 ± 4, {3.8 ± 0.8}	0.019 ± 0.004 {0.0070 ± 0.0017}	9.5 {19 ± 1}
16	(NH$_3$)$_4$	12.4;[f] {11.89}	11.45 {11.07}	22;[f] {39}	5.5 ± 1.7; {1.2 ± 0.4}	0.012 ± 0.004 {0.0047 ± 0.0015}	22; {39}

[a] $h\nu_{max}$(em), determined in butyronitrile (bun) or ethanol/methanol (alc; v/v′ = 4/1) solution. [b] Mean excited state decay rate constant, $k_{obs} = 1/\tau$. [c] Emission quantum yield; error bars based on replicate determinations. [d] $k_{RAD} = \phi k_{obsd}$. [e] $k_{NRD} = k_{obsd} - k_{RAD}$. [f] References 37, 38, and 66. [g] References 66 and 67. [h] Reference 23.

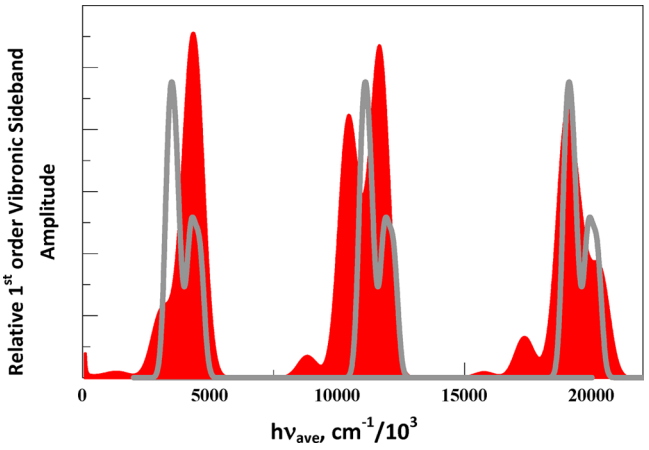

Figure 3. Contrasts in the expected variations in excited state distortions, as manifested in the first order $(FC)^2$ contributions to the $(M)^2$, for a $[Ru(NH_3)_4bpy]^{2+}$-like complexes at different energies assuming that $|\vec{M}| = |\vec{M}|_{el}(FC)$ with (a; red) and without (b; gray) configurational mixing. The calculated first-order vibronic contributions are based on (a) DFT-modeled emission sideband contributions[20] (red curves; progressions in single vibrational modes, $\sum_{k=1}^{all}\sum_{j=1}^{\infty}(FC)_{j,k}^2$); and (b), $\sum_{k=1}^{all}(FC)_{j=1,k}^2$ and eqs 10−15 using resonance-Raman parameters[53] (gray curves). The DFT-modeled sideband amplitudes were obtained by dividing the intensities of the progressions in first-order distortion modes by $(h\nu_{em})^4$;[64] see discussion in the text. The amplitudes of the vibronic features at about 19 000 cm^{-1} of the two modeling approaches were adjusted to be the same for $h\nu_{max}$(emis) ≈ 19 000 cm^{-1} ($h_{0'0}$ = 20 500 cm^{-1}).

the effects of configurational mixing on the excited state distortions.

Table 2. Resonance-Raman Parameters Reported for $[Ru(NH_3)_4bpy]^{2+}$[53]

distortion modes			
low frequency		medium frequency	
ν_k, cm^{-1}	S_k	ν_k, cm^{-1}	S_k
456	0.036	1605	0.072
376	0.328	1548	0.065
248	0.106	1481	0.151
667	0.192	1331	0.084
		1260	0.011
		1172	0.045
		1027	0.051

The comparison in Figure 3 is of the vibronic (or Franck−Condon) amplitudes for two different conceptual models, and the resulting bandshapes should not be significantly dependent on ν_m^3, as, in eq 3, results are dependent on $h\nu_m$. However, this is assuming that the calculated intensities depend on vibronic progressions whose amplitudes are linearly dependent on ν_m. The Gaussian code used to calculate the emission intensities does contain a factor of $h\nu_m$ in addition to the expected ν_m^3 factor. Dividing the calculated intensities of the first order progressions by $(h\nu_m)^4$ recovers the Franck−Condon terms, which are plotted as the red curves of Figure 3, whose integrated intensities are nearly independent of emission energy, as is expected for the Franck−Condon contributions; there is a weak energy dependence of these progressions that is presumably a consequence of the excited state/excited state configurational mixing and the resulting variations in bandshapes. Note that the DFT modeling results in large changes in the vibronic bandshapes and in relative component

DOI: 10.1021/jp510949x
J. Phys. Chem. B 2015, 119, 7393−7406

vibronic amplitudes, neither of which would occur in the absence of mixing with other electronic states (modeled by the gray curves in Figure 3) where the electronic distributions in the ^{3}MLCT excited states were the same at all energies; the changes in band shape in the DFT-modeled spectra have been attributed to mixing between different diabatic states.[20] It is noted that spectral intensities are expected to decrease as the excited state energy decreases since the higher energy vibronic components (usually harmonics and combination bands) contributing to (FC) can only contribute when their energies are smaller than the excited state energy. This decrease in contributions of the highest energy harmonics is evident in the single mode progressions in Figure 3. It is important to observe that the calculations of the Franck−Condon factors and the distortions using the Gaussian program do not have intrinsic energy dependences.

The comparison of vibronic amplitudes in Figure 3 differs from the comparisons in Figures 3−7 of our previous work,[20] in which calculated intensity values, instead of the Franck−Condon amplitudes, were used to compute the vibrationally resolved emission spectra for Ru-bpy complexes. Thus, Figure 3 in the work of Lord et al.,[20] corrected for the energy dependence of the calculated $[Ru(NH_3)_4bpy]^{2+}$ spectrum, would increase the relative magnitude calculated for the dominant vibronic sideband to about 70% of that of the emission maximum, which is very close to the observed ratio. Similarly, Figures 5 and 6 compare the amplitudes of the resonance-Raman (rR) vibronic components for $[Ru(NH_3)_4bpy]^{2+}$ with the DFT-calculated intensity results and correction for the energy dependence of the DFT calculated intensities brings the amplitudes of the curves that convolute the low ($h\nu_{vib}$ < 750 cm^{-1}) and medium frequency modes into much better agreement with the resonance-Raman data.

2. Triplet Manifold Modeling by DFT for Selected Complexes. Many ruthenium complexes have one or more triplet metal centered excited states (^{3}MC) with energies near[23] or lower than[21] that of the lowest energy ^{3}MLCT excited state, and this proximity in energy can result in a shorter ^{3}MLCT excited state lifetime and/or a possible value of γ < 1, thereby complicating the evaluation of k_{RAD} from eq 6. We used DFT modeling of the low energy triplet states in order to identify such complexes in order to exclude them from our k_{RAD} correlations. Most of the complexes reported here have the ^{3}MLCT state as the lowest energy triplet excited state (T_0) and the metal-centered ^{3}MC states higher in energy by about 2100−4200 cm^{-1}. Among the complexes studied, $[Ru([9]aneS_3)(CN)(bpy)]^+$ and $[Ru(NCCH_3)_2(bpy)_2]^{2+}$ are high energy emitters, while $[Ru(en)(bpy)_2]^{2+}$, $[Ru(NH_3)_2(bpy)_2]^{2+}$, $[Ru(O_4C_2)(bpy)_2]$, and $[Ru([14]aneN_4)(bpy)]^{2+}$ complexes emit at lower energies (Table 1). The ^{3}MLCT and ^{3}MC states are approximately isoenergetic for $[Ru([14]aneN_4)(bpy)]^{2+}$ complex, and the ^{3}MC state is calculated to be about 1400 cm^{-1} lower in energy than the ^{3}MLCT state for the $[Ru([9]aneS_3)(CN)(bpy)]^+$ complex. For these complexes either internal conversion or the efficiency of forming the emitting state (γ) may complicate the estimation of k_{RAD} as discussed previously for other systems with $E(^3MC) \leq E(^3MLCT)$.[21,23] Consequently, we have not included them in the comparisons below. We failed to locate a bound ^{3}MC state for the $[Ru(NCCH_3)_2(bpy)_2]^{2+}$ complex. All of our attempts led to the dissociation of one of the CH_3CN ligands showing that the molecule is prone to photodissociation following ^{3}MLCT to ^{3}MC internal conversion. The energy of a dissociative state is not well-defined, and we have not included this complex in our comparisons. It should be noted that the apparent values of $k_{RAD} = [(\phi_{em}/\gamma) \times k_{obsd}]$ (based on eq 6) for the $[Ru([14]aneN_4)(bpy)]^{2+}$ and $[Ru([9]aneS_3)(CN)(bpy)]^+$ complexes are well below those of shown in the correlations of Figures 6 and 7.

Table 3. Calculated Relative Energies (ΔE_{SCF} in cm^{-1}) of the ^{3}MLCT and ^{3}MC States on the Triplet Manifold for Selected $[Ru(L)_{6-2n}(bpy)_n]^{2+}$ Complexes

$(L)_{6-2n}$	^{3}MLCT	^{3}MC
$([9]aneS_3)(CN^-)$	0.0 (T_1)	−1360(T_0)
$(bpy)(NCCH_3)_2$	0.0	dissociative (T_0)
(bpy)(en)	0.0 (T_0)	2060(T_1)
$(bpy)(NH_3)_2$	0.0 (T_0)	2000(T_1)
$(bpy)(O_4C_2)$	0.0 (T_0)	4060 (T_1)
$([14]aneN_4)$	0.0	−105
$(NH_3)_4$	0.0 (T_0)	2980(T_1) 3500 (T_2)

Mulliken spin density values on the Ru atom are reported for all the triplet excited states (Figure 4), validating the convergence to the desired electronic states. A lower than expected spin density value in the ^{3}MLCT states of $[Ru([9]aneS_3)(CN)(bpy)]^+$ and $[Ru(O_4C_2)(bpy)_2]$ complexes is a result of delocalization of some charge onto the cyanide and oxalate moieties, respectively. The coordination sphere distortions in the ^{3}MC states are also depicted in Figure 4. For most of the complexes, the distortion is found along one of the N(bpy)−Ru−ligand axis. In the ^{3}MC state of $[Ru([9]aneS_3)(CN)(bpy)]^+$, Ru−$S_1$ and Ru−N6 bond lengths are elongated to 2.64 and 2.50 Å from their respective distances, 2.39 and 2.08 Å in the ^{3}MLCT state. The distortions from ^{3}MLCT to ^{3}MC states are found to be similar in $[Ru(en)(bpy)_2]^{2+}$ and $[Ru(NH_3)_2(bpy)_2]^{2+}$ complexes: internal conversion results in elongation of the Ru−N_6(bpy) bond by 0.39 and 0.36 Å, while the Ru−N_3 bond is found to elongate by 0.42 and 0.43 Å, respectively. In the case of $[Ru(O_4C_2)(bpy)_2]$, the ^{3}MLCT/^{3}MC difference in the Ru−O_3 bond lengths is 0.25 Å and hence smaller than that found for the Ru−N bond length differences in $[Ru(am(m)ine)_2(bpy)_2]^{2+}$ complexes. This contrast correlates with the negative charge present on the oxygen atom of oxalate, but stereochemical constraints imposed by the oxalate ligand could also contribute. Elongation of the Ru−N(cyclam) bonds from ^{3}MLCT to ^{3}MC state is calculated to be 0.10−0.32 Å for $[Ru([14]aneN_4)(bpy)]^{2+}$ complex while the Ru−N(ammine) bonds are found to be more elongated 0.41−0.45 Å in the case of $[Ru(NH_3)_4(bpy)]^{2+}$. This can be attributed to the stereochemical constraints imposed by the macrocyclic $[14]aneN_4$ ligand.

3. Contributions of the bpy Ligand to the "Metal-Centered" Singly Occupied Molecular Orbital (SOMO) of the ^{3}MLCT Excited States. Figure 5 shows the calculated SOMOs of the triplet MLCT excited states for a number of Ru-complexes. SOMO 1 is Ru(d_π)-based, while SOMO 2 is a π^* MO on the bpy ligand. As illustrated in the figure, "metal-centered" SOMO 1 has a contribution from the π-orbital of bpy ligand for all the complexes. SOMO 1 of $[Ru([14]aneN_4)(bpy)]^{2+}$, $[Ru(NH_3)_2(bpy)_2]^{2+}$, and $[Ru(en)(bpy)_2]^{2+}$ species has 89%, 87%, and 86% Ru(d_π) contribution, respectively. These results illustrate that SOMO 1 is not a pure metal-centered orbital but has contributions from the bpy ligand. The corresponding SOMO for $[Ru(ox)(bpy)_2]$ species is 81% and

DOI: 10.1021/jp510949x
J. Phys. Chem. B 2015, 119, 7393−7406

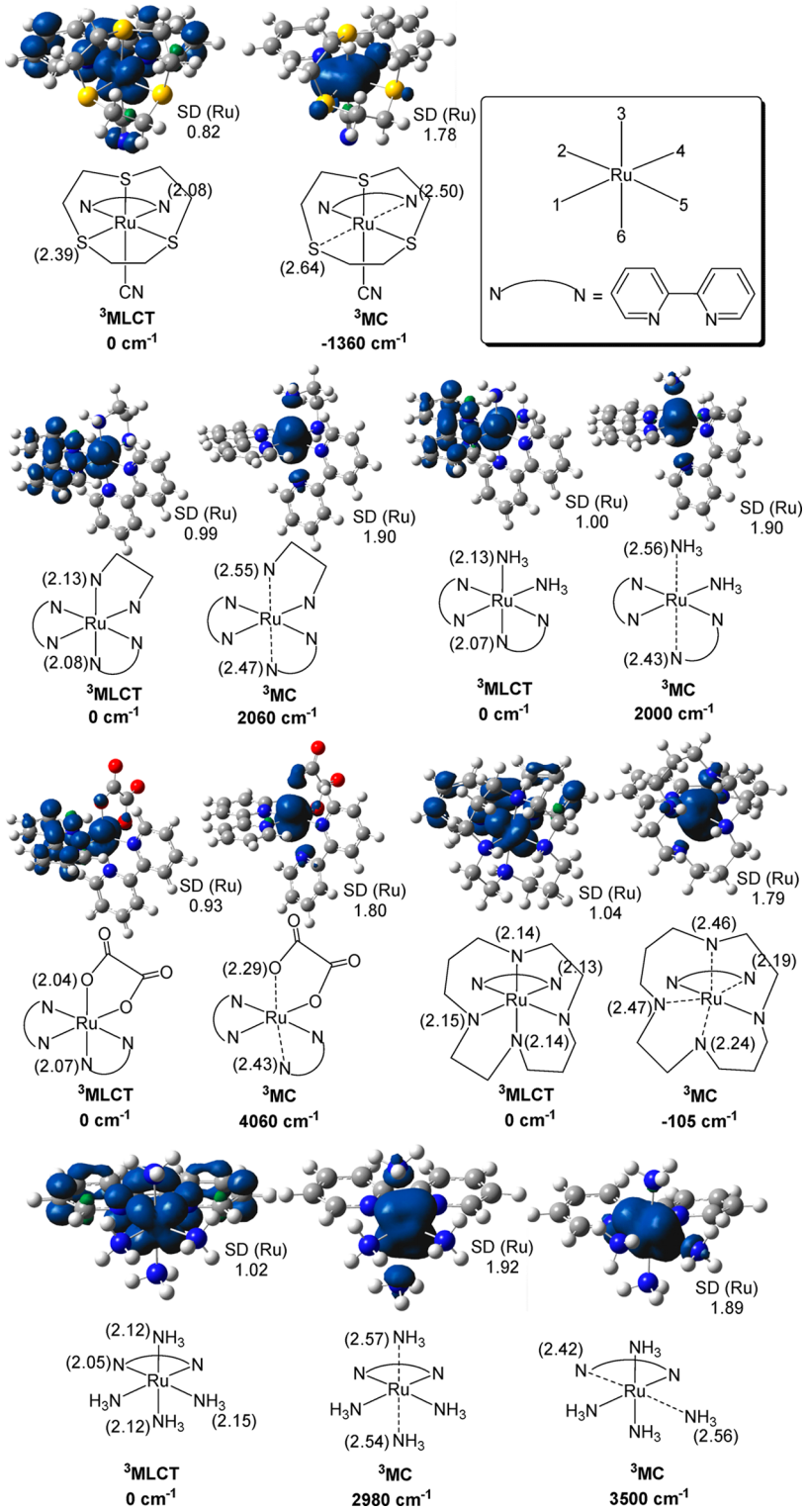

Figure 4. Spin density (SD) plots (isosurface value 0.004 au) and geometries of the lowest energy triplet excited states for selected complexes. Values in parentheses are relevant bond distances (in Å) illustrating the differences in the ^{3}MC and ^{3}MLCT Ru−L bond lengths.

6% in Ru(d_π) and ox(p_π) character, respectively, while the rest is contributed by the bpy ligand. The Ru(d_π) character calculated for SOMO 1 of $[Ru(NCCH_3)_2(bpy)_2]^{2+}$ and $[Ru([9]aneS_3)(CN)(bpy)]^+$ species is considerably lower 77% and 70%, respectively, compared to those of the other complexes. The π-orbitals of the CH_3CN ligands contribute by about 4% in $[Ru(NCCH_3)_2(bpy)_2]^{2+}$ and the π-orbitals of the cyano and sulfur ligands contribute by about 9% in SOMO 1 of $[Ru([9]aneS_3)(CN)(bpy)]^+$. Therefore, the contribution of the bpy ligand for these two complexes is found to be highest about 20% when compared among the other species studied which is consistent with the fact that $[Ru(NCCH_3)_2(bpy)_2]^{2+}$ and $[Ru([9]aneS_3)(CN)(bpy)]^+$ are found to be the highest energy emitters among the complexes in Table 1. The above results

DOI: 10.1021/jp510949x
J. Phys. Chem. B 2015, 119, 7393−7406

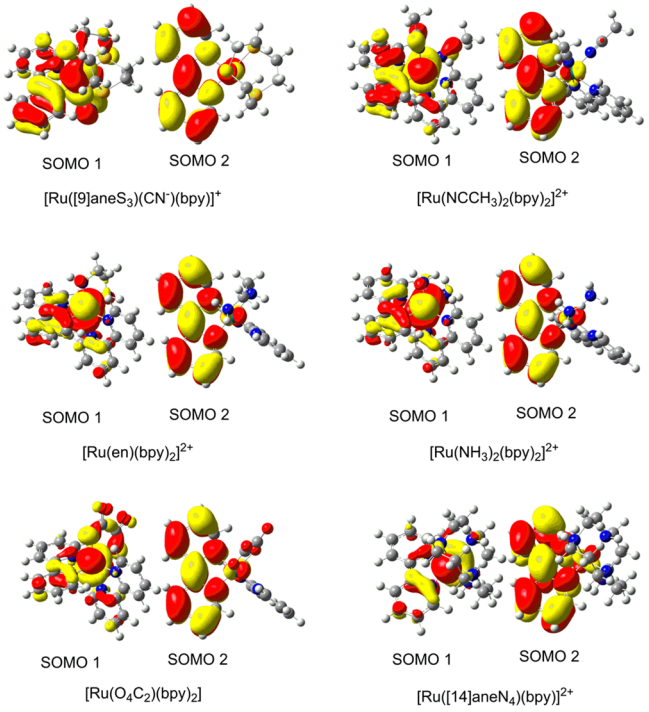

Figure 5. Biorthogonalized singly occupied molecular orbitals (SOMOs with an isosurface value of 0.02 au) of the ^{3}MLCT states for selected complexes. The "metal-centered" SOMO (SOMO 1) has contribution from the π-orbital of bpy for all the complexes, which illustrates that the emissive triplet state is not a pure metal-to-ligand charge transfer state; instead it has a component from one of the higher energy bpy-based excited states.

suggest that, for all the complexes studied, the emissive state is not a pure metal-to-ligand charge transfer state but it is mixed with a higher energy bpy-based excited state. It is also noteworthy that SOMO 2 has a very small (2−3%) Ru-(d-orbital) contribution that remains constant for the complexes studied.

4. Variations in the ^{3}MLCT State Distortions of Ru−N(bpy) Bond Distances and Contributions from the bpy Ligand Orbitals. The largest distortions of the ^{3}MC excited states are usually found to be along an L−Ru−L′ axis or, in a few cases, in a Cartesian plane (analogous to the Jahn−Teller distortions in the octahedral limit)[82,83] so that the interpretation of individual bond length variations is not simple; however, there do appear to be some patterns that are consistent with the general implications of our observations. Table 4 contains the average Ru−N(bpy) bond lengths calculated from Ru−N_1 and Ru−N_2 distances in the S_0 and ^{3}MLCT states for a number of mono-bpy complexes. The difference in the average Ru−N(bpy) bond lengths between those two states (Δ in Table 4) should be a function of (a) the variations in electrostatic attraction between the negatively charged ligand and the positively charged metal; (b) variations in the covalent interactions between the metal and ligand; and (c) stereochemical constraints imposed by the coordinated ligands. The charge on the metal is the effective nuclear charge and tends to increase as the excited state energy increases, while the charge on the ligand appears to vary less; if this were the dominant factor, Δ would be expected to increase (or the excited state bond length to decrease) as the ^{3}MLCT energy increases (the order of increasing bpy ligand character in this SOMO), contrary to the observations in Table 4: the calculations indicate that Δ increases along the series of

Table 4. Differences in the Ru−N(bpy) Bond Lengths (in Å) between Ground S_0 and Excited ^{3}MLCT States for Selected Complexes

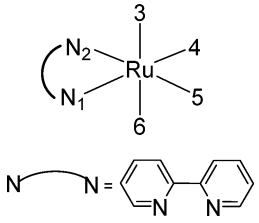

	S_0 $(Ru-N)_{avg}$[a]	^{3}MLCT $(Ru-N)_{avg}$[a]	Δ (^{3}MLCT-S_0)
([9]aneS$_3$)(CN$^-$)	2.10	2.05	−0.05
(bpy)(NCCH$_3$)$_2$	2.07	2.04	−0.03
(bpy)(en)	2.07	2.06	−0.01
(bpy)(NH$_3$)$_2$	2.07	2.05	−0.02
(bpy)(O$_4$C$_2$)	2.05	2.06	0.01
([14]aneN$_4$)	2.10	2.11	0.01

[a] $(Ru-N)_{avg}$ is calculated from Ru−N(bpy) distances as (Ru−N_1 + Ru−N_2)/2.

[Ru([14]aneN$_4$)(bpy)]$^{2+}$, [Ru(O$_2$C$_4$)(bpy)$_2$], [Ru(NH$_3$)$_2$(bpy)$_2$]$^{2+}$, [Ru(en)(bpy)$_2$]$^{2+}$, [Ru(NCCH$_3$)$_2$(bpy)$_2$]$^{2+}$ and [Ru([9]aneS$_3$)(CN)(bpy)]$^+$ complexes with the largest values of Δ for the latter two complexes, 0.03 and 0.05 Å, respectively. On the other hand, the amount of bpy ligand character in donor SOMO for the latter two complexes is also the largest, suggesting that the (weak) excited state covalent bonding interaction between the bpy(π) and the Ru(dπ-hole) is largest for [Ru(NCCH$_3$)$_2$(bpy)$_2$]$^{2+}$ and [Ru([9]aneS$_3$)(CN)(bpy)]$^+$. Since all of the ^{3}MLCT excited states involve a single bpy acceptor, there should be little variation in stereochemical effects through this series of complexes. This is consistent with the general inference that the highest energy emitters have their emissive ^{3}MLCT states strongly mixed with a higher energy bpy-based excited electronic excited state.

C. Excited State Energy Dependence of k_{RAD}. Figure 6 compares the observed values of k_{RAD} (based on eq 6 with γ = 1.0) on a scale suggested by eq 3 and indicates that k_{RAD} is not as simply dependent on $(h\nu_{ave})^3$ as suggested by that equation. Statistically comparable fits of the experimental observations are obtained with either the cubic (per eq 3) or linear (per eq 4; Supporting Information Figure S3A) energy dependencies of k_{RAD} on $h\nu_{ave}$. The observed energy dependence either requires an intercept on the x-axis or that the dependence for $h\nu_{ave}$ < 10 000 cm^{-1} is much weaker than that for $h\nu_{ave}$ > 10 000 cm^{-1}. The apparent intercept for a linear fit of the data in Figure 6 is best interpreted as being determined by $(\overrightarrow{M_{D^+A^-}})^2 \approx (\alpha_{CT,IL}\overrightarrow{M_{IL}})^2$ in eq 5, where the additional energy dependence (shown in Figure 7) arises from the mixing coefficient, $\alpha_{CT,IL} \approx (H_{CT,IL})/(E_{IL} - E_{CT})$, and only contributes significantly for $E_{IL} \geq h\nu_m \geq E_{CT}$. Such a very weak energy dependence for $h\nu_{ave}$ < 10 000 cm^{-1} is consistent with eq 5. Equation 5 is the simplest and most appropriate available approach for describing the transition dipole and, thereby, k_{RAD} in these systems.

The scatter of experimental data in Figure 6 is appreciable, with much of it the result of errors in the determination of low temperature absorptivities for the quantum yield measurements (replicate determinations had mean errors in the range of 15−20%). There may also be some systematic sources of the scatter. Thus, the ancillary ligands contribute to the donor

DOI: 10.1021/jp510949x
J. Phys. Chem. B 2015, 119, 7393−7406

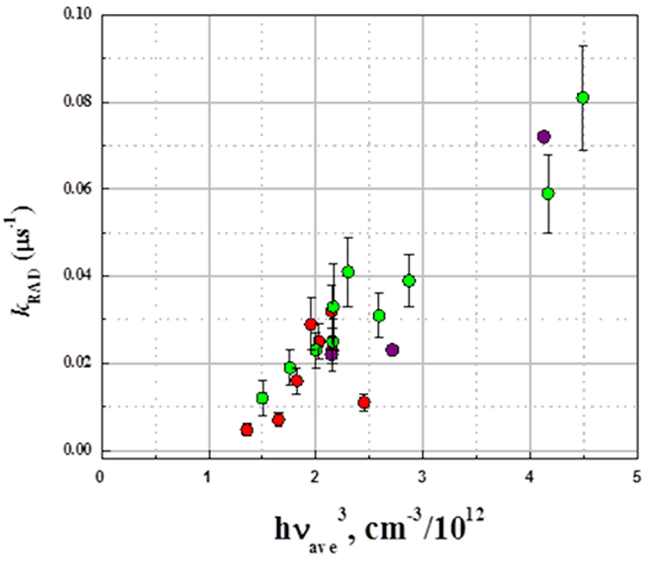

Figure 6. Comparison of the observed radiative rate constants (circles) with $(h\nu_{ave})^3$ for complexes with $E(^3MC) > E(^3MLCT)$, where $k_{RAD} = (\phi_{em}/\gamma)k_{obsd}$ and $\gamma = 1.0$. Green circles, in butyronitrile; red circles, in alcohol; purple circles, Demas and Crosby data in alcohol (see Table 1).[66] A least-squares line can be drawn through the experimental data with ($r^2 = 0.82$): $k_{RAD} = (2.2 \pm 0.02) \times 10^{-4}$ $(h\nu_{ave})^3 - 0.022 \pm 0.005$ s^{-1} (for $h\nu_{ave}$ in $cm^{-1}/10^3$); the apparent x-axis intercept corresponds to $h\nu_{ave}$ 10 700 ± 3700 cm^{-1}. See Table 1 and Supporting Information Figure S3C for identity of the complexes. Error bars indicate the average deviations of replicate determinations.

properties of the lowest energy ^{3}MLCT excited state for some complexes (e.g., for L = Cl^- and $C_2O_4^{2-}/2$) sometimes giving rise to unique ancillary ligand distortions and the stereochemical constraints imposed by some ancillary ligands limit the extent of Ru-L distortions. For example, our DFT modeling indicates that the Ru−N(ane) distortions are stereochemically restricted in $[Ru([14]aneN_4)(bpy)]^{2+}$, which would lead to relatively smaller amplitude vibronic contributions than found in the less encumbered complexes.

Equation 5 suggests that the correlation in Figure 6 should be nonlinear with an intercept that is determined by its first term (which is equal to eq 3; see also eq 19 below). However, the possibility that the apparent intercept for a linear fit of $(\phi_{em}/\gamma)k_{obsd}$ in Figure 6 somehow originates from values of $\gamma <$ 1 in eq 6 should also be considered.[84] In considering this possibility, it should first be observed that (a) several of the apparent emission quantum yields for complexes in the high energy regime are in the range of 0.5 ± 0.2, so that for these complexes γ must be greater than or equal to 0.3 and if this were universally the case for the complexes included in the correlation, then the correction for the effect would change the slope of any apparent correlation line (note that from eq 6, $k_{RAD} = (\phi_{em}/\gamma)k_{obsd}$), but it would not change the value of the intercept; and (b) $\gamma = 1.0$ has been determined for the $[Ru(bpy)_3]^{2+}$ complex[85] which is one of the complexes in the correlation. In view of these considerations, the only way that the values of $\gamma < 1$ could account for the apparent nonzero intercept in Figure 6 would be if γ were to decrease systematically with decreasing ^{3}MLCT excited state energy, and there is no basis for expecting such behavior. In addition, a systematic decrease of $\gamma < 1$ with energy would result in a weaker than expected and nonlinear dependence of ln k_{NRD} on energy, whereas the assumption that $\gamma = 1$ for the complexes with $E(^3MLCT) < E(^3MC)$ results in a plausible linear dependence of ln k_{NRD} on energy as expected[27] (see Figure S3C in the Supporting Information).[81] On the other hand, we have found that many complexes for which a ^{3}MC state has a (calculated) energy that is less than or equal to the (calculated) energy of the lowest energy ^{3}MLCT excited state tend to have values of k_{RAD} that are smaller than those expected based on correlations such as that in Figure 6; see Table 2 and our previous reports.[21,23] This behavior can arise from either (1) multiple upper state relaxation channels leading to inefficient population of the emitting state ($\gamma < 1$ in eq 6); and/or (2) a contribution of k_{IC} to k_{obs}.[21,23] Consequently, we have not used the values of k_{RAD} for systems for which DFT modeling indicates that $E(^3MLCT) > E(^3MC)$ in the comparisons in Figures 6 and 7. Some of the complexes with $E(^3MC) \leq E(^3MLCT)$ emit very strongly (Tables 1 and 3 and ref 21), and this "non-Kasha" behavior[28,86] probably arises in these complexes because the distortions in the ^{3}MC excited states are so much larger and in different vibrational modes than those of the ^{3}MLCT excited states that the nuclear reorganizational energy barriers to internal conversion can be very large compared to k_BT at 77 K.[21] These issues are currently being further investigated.

We have attempted to find well behaved Ru-bpy chromophores with emission maxima at relatively high energies, but the DFT modeling of complexes with $h\nu_{max}(MLCT) \geq$ ~17 000 cm^{-1} has consistently found that they have metal-centered excited states with lower energies than the emitting ^{3}MLCT excited states as discussed above and previously.[21] The very large metal−ligand distortions make a significant contribution to the energies of the ^{3}MC excited states of this class of complexes, and the preliminary observations[21,23] indicate that E(^{3}MC) tends to vary over a smaller energy range than does E(^{3}MLCT). Substrate photodecomposition at 77 K has complicated our attempts to determine k_{RAD} for some complexes with $h\nu_{max} >$ ~ 17 000 cm^{-1}, and seems to arise from the near-ultraviolet irradiation of the ^{3}MLCT transient excited states.[21]

DISCUSSION

The values of k_{RAD} that we have found suggest that the observed emissions of Ru-bpy ^{3}MLCT excited states gain much of their intensities from mixing with "local" bpy-ligand-centered, presumably $\pi\pi^*$(bpy), excited states in accord with the intensity stealing model that has been discussed by Mulliken and Person,[17] applied by Bixon, Jortner, and Verhoeven to some linked organic D/A complexes,[36] and as in eq 5. The observations are not in good accord with simpler (largely two state-based) approaches of eqs 3 and 4 that have been previously used to describe and interpret the emission spectra of these complexes. The details and implications of this work are discussed in the following.

Equation 3 indicates that a plot of k_{RAD} versus $(h\nu_{ave})^3$ should be linear and pass through the origin. However, Figure 6 shows that the experimental data seem to require an intercept of about 10 000 cm^{-1}. This behavior is consistent with eq 5 and suggests that a "pure" MLCT transition would only be observed at the very lowest excited state energies. Furthermore, the observed values of k_{RAD} appear to be largely the result of mixing between the ^{3}MLCT and $\pi\pi^*$(bpy) excited states, or based on eq 5 and setting IL = $\pi\pi^*$ for these complexes,

DOI: 10.1021/jp510949x
J. Phys. Chem. B 2015, 119, 7393−7406

$$k_{RAD} \approx C_i \nu^3 \eta^3 (M^2_{D^+A^-} + \alpha^2_{CT,\pi\pi^*} M^2_{\pi\pi^*})$$
$$\approx (h\nu_{ave})^3 A[(M^{dia}_{MLCT(el)})^2 (FC^{dia}_{MLCT})^2 + \alpha^2_{CT\pi\pi^*} (M^{dia}_{\pi\pi^*(el)})^2 (FC^{dia}_{\pi\pi^*})^2] \quad (19)$$

where the constant A is based on eqs 3 and 5, and the transition moments and Franck−Condon factors in the braces are those that correspond to a diabatic (dia) MLCT transition and from MLCT/$\pi\pi^*$ mixing, respectively. This interpretation amounts to "intensity stealing" by a very weak, "pure" MLCT transition from a strongly allowed transition localized on the acceptor ligand (note that $\pi\pi^*$(bpy) absorption bands are typically far more intense than MLCT absorptions). It is important to note that this interpretation is not included in the DFT modeling since the program used does not account for spin−orbit coupling or take account of the spin forbidden nature of the emission. In effect, the computational modeling allows for configurational mixing with any of the higher energy excited states with the same spin, so the actual amplitudes of the excited state distortions could be different. However, the trends and general intensity patterns are expected to be reasonably well described.

Equations 3 and 19 imply that dividing the data in Figure 6 by $(h\nu_{ave})^3$ should give a quantity proportional to M^2. For eq 3 the result should be independent of $h\nu_{ave}$, while for eq 5 there should be two relatively clearly separated regimes: one energy independent and one energy dependent. Figure 7 clearly shows

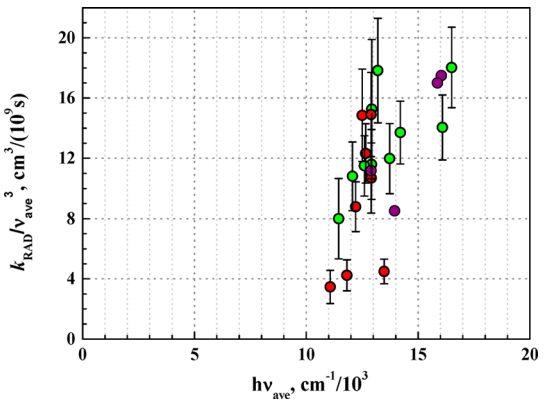

Figure 7. Comparison of the variations in (observed radiative rate constants) ÷ $(h\nu_{ave})^3$ (circles) with $h\nu_{ave}$ for the complexes shown in Figure 6. See caption of Figure 6 for color code and other details.

two different energy regions consistent with eqs 5 and 19, with the values of $k_{RAD}/(h\nu_{ave})^3$ increasing as excited state energy increases, and the approximately 5-fold increase is over a relatively small range (ca. 7000 cm^{-1}) of $h\nu_{ave}$.

Equations 5 and 19 are reasonably consistent with the rather abrupt rise in the experimental values of k_{RAD} with $h\nu_{ave}$. The spin density calculations imply that even for the complexes with the highest energy ^{3}MLCT excited states that we have examined ($h\nu_{0'0} \approx 19\,000$ cm^{-1}),[21,23] the $\pi\pi^*$ states are higher than the ^{3}MLCT state consistent with the studies of Nozaki and co-workers on $[Zn(bpy)_3]^{2+}$ that place the $\pi\pi^*$ states above 21 000 cm^{-1}.[87] As $E_{0'}(^3MLCT)$ or $h\nu_{ave}$ decreases, $\Delta E_{CT,\pi\pi^*} = E_{v'}(\pi\pi^*) - E_{0'}(^3MLCT)$ increases and $\alpha^2_{CT,\pi\pi^*} = ((H_{CT,\pi\pi^*})/(\Delta E_{CT,\pi\pi^*}))^2$ rapidly becomes small. Therefore, for small excited state energies, $E(^3MLCT) < 10\,000$ cm^{-1}, $\alpha_{CT,\pi\pi^*}$ should be negligible and eq 5 suggests that the values of k_{RAD} should approach those of "pure" ^{3}MLCT excited states with the values of M^2 nearly constant. The correlation in Figure 6 indicates that k_{RAD} should be very small for $E(^3MLCT) < 10\,000$ cm^{-1}. Complexes with ^{3}MLCT excited states in this low energy regime have been difficult to investigate since they generally involve anionic, oxidizable ligands such as halides, which also contribute to the HOMO and often make the Ru^{II} excited state strongly reducing.[85]

CONCLUSIONS

This work strongly supports our recent inference that the emission bandshapes of Ru-bpy chromophores are functions of configurational mixing between the ^{3}MLCT and higher energy $\pi\pi^*$ excited states of the bpy ligand.[20] Some implications of the present work are (a) a "pure" Ru-bpy ^{3}MLCT excited state is not greatly distorted and that its emission has weak vibronic contributions in the region of bpy-ligand vibrational modes; (b) a "pure" Ru-bpy ^{3}MLCT emission has a very small radiative rate constant; and (c) we have no evidence that a "pure" Ru-bpy ^{3}MLCT emission has yet been observed. The energy dependence of the radiative rate constants discussed here has contributions in addition to the classical $(h\nu)^3$ dependence (eq 3), and these contributions most likely arise from configurational mixing with a higher energy excited state of the system, probably a bpy-ligand $\pi\pi^*$ excited state. There are many features of this mixing that are as yet uncertain, but apparently the decay of a "pure" ^{3}MLCT excited state to the singlet ground state is strongly forbidden, and it seems likely that the excited state/excited state mixing is promoted by spin−orbit coupling with an excited state which relaxes the forbiddeness of the ^{3}MLCT/S_0 transition and gives rise to much or most of the observed vibronic structure. The upper state that is most readily related to our observations is one whose energy is independent of the charge transfer (or donor/acceptor) parameters, and this has led us to identify it with the very strongly allowed $^1\pi\pi^*$(bpy) transition. Our observations do not require that the $^1\pi\pi^*$(bpy) and ^{3}MLCT states mix directly, and other states (such as ^{1}MLCT, $^3\pi\pi^*$, etc.) may be involved. In very qualitative terms, the CT/$\pi\pi^*$ mixing adds some of the $\pi\pi^*$ properties, including distortions and Franck−Condon factors, to the forbidden diabatic MLCT transition. Thus, the mixing provides a mechanism through which the spin forbidden ^{3}MLCT → S_0 transition gains intensity, and this gain in intensity is accompanied by vibronic components characteristic of the strongly allowed intense transition.

ASSOCIATED CONTENT

Supporting Information

Electrochemistry of complexes; ambient absorption, 90 K absorption and 77 K emission parameters; energy dependence of k_{RAD}; cubic energy dependence of k_{RAD}; XYZ coordinates of DFT-calculated structures; skeletal structure of Ru(tpm)(bpy)-$(NCCH_3)]^{2+}$; cyclic voltammogram of $[Ru(tpm)(bpy)-(NCCH_3)]^{2+}$; emission spectra of the $[Ru(NH_3)_4(bpy)]^{2+}$, $[Ru(en)_2(bpy)]^{2+}$ and *mer*-$[Ru(NH_3)_3(bpy)(L)]^{2+}$ series; 298 K absorption of $[Ru(tpm)(bpy)(NCCH_3)](PF_6)_2$ in acetonitrile. This material is available free of charge via the Internet at http://pubs.acs.org.

AUTHOR INFORMATION

Notes

The authors declare no competing financial interest.

DOI: 10.1021/jp510949x
J. Phys. Chem. B 2015, 119, 7393−7406

■ ACKNOWLEDGMENTS

Marshall Newton's published and private communications have long challenged and guided our work. His comments on the material presented here have been very helpful in the evolution of our arguments, and we are grateful to him for providing several key references. This work was funded in part (J.F.E. and H.B.S.) by the Division of Chemical Sciences, Geosciences, and Biosciences, Office of Basic Energy Sciences of the U.S. Department of Energy through Grant DE-FG02-09ER16120; and in part (Y.J.C.) by the Ministry of Science and Technology (Taiwan, R.O.C) through Grants NSC 101-2113-M-030-005.

■ REFERENCES

(1) Graetzel, M. Solar Energy Conversion by Dye-Sensitized Photovoltaic Cells. *Inorg. Chem.* **2005**, *44*, 6841−6851.
(2) Graetzel, M.; Moser, J.-E. In *Electron Transfer in Chemistry*; Balzani, V., Ed.; Wiley-VCH: Weinheim, Germany, 2001; Vol. *5*, p 589.
(3) Alstrum-Acevedo, J. H.; Brennaman, M. K.; Meyer, T. J. Chemical Approaches to Artificial Photosynthesis. 2. *Inorg. Chem.* **2005**, *44*, 6802−6827.
(4) Balzani, V.; Credi, A.; Venturi, M. Photochemistry and photophysics of coordination compounds: An extended view. *Coord. Chem. Rev.* **1998**, *171*, 3−16.
(5) Balzani, V.; Juris, A.; Venturi, M.; Campagna, S.; Serroni, S. Luminescent and Redox-Active Polynuclear Transition Metal Complexes. *Chem. Rev.* **1996**, *96*, 759−834.
(6) *Supramolecular Photochemistry*; Balzani, V., Scandola, F., Eds.; Horwood: Chichester, U.K., 1991.
(7) Barbara, P. F.; Meyer, T. J.; Ratner, M. Contemporary Issues in Electron Transfer Research. *J. Phys. Chem.* **1996**, *100*, 13148−13168.
(8) Lewis, N. S. Chemical Control of Charge Transfer and Recombination at Semiconductor Photoelectrode Surfaces. *Inorg. Chem.* **2005**, *44*, 6900−6911.
(9) Lewis, N. S.; Nocera, D. G. Powering the Planet: Chemical Challenges in Solar Energy Utilization. *Proc. Natl. Acad. Sci. U.S.A.* **2006**, *103*, 15729−15735.
(10) Bignozzi, C. A.; Argazzi, R.; Boaretto, R.; Busatto, E.; Carli, S.; Ronconi, F.; Caramori, S. The Role of Transition Metal Complexes in Dye Sensitized Solar Devices. *Coord. Chem. Rev.* **2013**, *257*, 1472−1492.
(11) Ondersma, J. W.; Hamann, T. W. Recombination and Redox Couples in Dye-Sensitized Solar Cells. *Coord. Chem. Rev.* **2013**, *257*, 1533−1543.
(12) Manbeck, G. F.; Brewer, K. J. Photoinitiated Electron Collection in Polyazine Chromophores Coupled to Water Reduction Catalysts for Solar H_2 Production. *Coord. Chem. Rev.* **2013**, *257*, 1660−1675.
(13) Endicott, J. F. In *Electronic Structure and Spectroscopy of Inorganic Compounds*; Solomon, E. I., Lever, A. B. P., Eds.; Wiley: New York, 1999; Vol. *2*, p 291.
(14) Endicott, J. F. In *Electron Transfer in Chemistry*; Balzani, V., Ed.; Wiley-VCH: New York, 2001; Vol. *1*, p 238.
(15) Gorelsky, S. I.; Kotov, V. Y.; Lever, A. B. P. Vertical Ionization Energies and Electron Affinities of Ions in Solution from Outer-Sphere Charge Transfer Transition Energies. *Inorg. Chem.* **1998**, *37*, 4584−4588.
(16) Lever, A. B. P.; Dodsworth, E. S. In *Electronic Structure and Spectroscopy of Inorganic Compounds*; Lever, A. B. P., Solomon, E. I., Eds.; Wiley: New York, 1999; Vol. *II*, p 227.
(17) Mulliken, R. S.; Person, W. B. *Molecular Complexes*; Wiley-Interscience: New York, 1967.
(18) Creutz, C.; Newton, M. D.; Sutin, N. Metal—Ligand and Metal—Metal Coupling Elements. *J. Photochem. Photobiol. A: Chem.* **1994**, *82*, 47−59.
(19) Allard, M. M.; Odongo, O. S.; Lee, M. M.; Chen, Y.-J.; Endicott, J. F.; Schlegel, H. B. Effects of Electronic Mixing in Ruthenium(II) Complexes with Two Equivalent Acceptor Ligands. Spectroscopic, Electrochemical, and Computational Studies. *Inorg. Chem.* **2010**, *49*, 6840−6852.
(20) Lord, R. L.; Allard, M. M.; Thomas, R. A.; Odongo, O. S.; Schlegel, H. B.; Chen, Y.-J.; Endicott, J. F. Computational Modeling of the Triplet Metal-to-Ligand Charge-Transfer Excited-State Structures of Mono-Bipyridine−Ruthenium(II) Complexes and Comparisons to their 77 K Emission Band Shapes. *Inorg. Chem.* **2013**, *52*, 1185−1198.
(21) Mazumder, S.; Thomas, R. A.; Lord, R. L.; Schlegel, H. B.; Endicott, J. F. A Density Functional Theory and Spectroscopic Study of Intramolecular Quenching of Metal-to-Ligand Charge-Transfer Excited States in Some Monobipyridine Ruthenium(II) Complexes. *Can. J. Chem.* **2014**, *92*, 996−1009.
(22) Tsai, C.-N.; Allard, M. M.; Lord, R. L.; Luo, D.-W.; Chen, Y.-J.; Schlegel, H. B.; Endicott, J. F. Characterization of Low Energy Charge Transfer Transitions in (terpyridine)(bipyridine)Ruthenium(II) Complexes and Their Cyanide-Bridged Bi- and Tri-Metallic Analogues. *Inorg. Chem.* **2011**, *50*, 11965−11977.
(23) Tsai, C.-N.; Tian, Y.-H.; Shi, X.; Lord, R. L.; Luo, D.-W.; Schlegel, H. B.; Endicott, J. F.; Chen, Y.-J. Experimental and DFT Characterization of Metal-to-Ligand Charge-Transfer Excited States of (Rutheniumammine)(Monodentate Aromatic Ligand) Chromophores. *Inorg. Chem.* **2013**, *52*, 9774−9790.
(24) Gould, I. R.; Noukakis, D.; Gomez-Jahn, L.; Young, R. H.; Goodman, J. L.; Farid, S. Radiative and Nonradiative Electron Transfer in Contact Radical-Ion Pairs. *Chem. Phys.* **1993**, *176*, 439−456.
(25) Endicott, J. F.; Chen, Y. J. Electronic Coupling Between Metal Ions in Cyanide-Bridged Ground State and Excited State Mixed Valence Complexes. *Coord. Chem. Rev.* **2013**, *257*, 1676−1698.
(26) Birks, J. B. *Photophysics of Aromatic Molecules*; Wiley-Interscience: New York, 1970.
(27) Englman, R.; Jortner, J. The Energy Gap Law for Radiationless Transitions in Large Molecules. *J. Mol. Phys.* **1970**, *18*, 145−164.
(28) Kasha, M. Characterization of Electronic Transitions in Complex Molecules. *Discuss. Faraday Soc.* **1950**, *9*, 14−19.
(29) Sun, Q.; Mosquera-Vazquez, S.; Daku, L. M. L.; Guénée, L.; Goodwin, H. A.; Vauthey, E.; Hauser, A. Experimental Evidence of Ultrafast Quenching of the ^{3}MLCT Luminescence in Ruthenium(II) Tris-bipyridyl Complexes via a ^{3}dd State. *J. Am. Chem. Soc.* **2013**, *135*, 13660−13663.
(30) Fabian, R. H.; Klassen, D. M.; Sonntag, R. W. Synthesis and Spectroscopic Characterization of Ruthenium and Osmium Complexes with Sterically Hindering Ligands. 3. Tris Complexes with Methyl- and Dimethyl-Substituted 2,2′-bipyridine and 1,10-phenanthroline. *Inorg. Chem.* **1980**, *19*, 1977−1982.
(31) Juris, A.; Balzani, V.; Barigelletti, F.; Compagna, S.; Belser, P. l.; Zelewsky, A. V. Ru(II) Polypyridine Complexes: Photophysics, Photochemistry, Eletrochemistry, and Chemiluminescence. *Coord. Chem. Rev.* **1988**, *84*, 85−277.
(32) Brunold, T. C.; Gudel, H. U. In *Inorganic Electronic Structure and Spectroscopy*; Solomon, E. I., Lever, A. B. P., Eds.; Wiley-Interscience: New York, 1999; Vol. *1*, p 259.
(33) Hush, N. S. Homogeneous and Heterogeneous Optical and Thermal Electron Transfer. *Electrochim. Acta* **1968**, *13*, 1005−1023.
(34) Flint, C. D. Intensities of Vibronic Origins in the Electronic Spectra of Amino and Aquo Coordination Complexes. *J. Chem. Soc., Faraday Trans. II* **1976**, *72*, 721−723.
(35) Zou, L.-Y.; Cheng, Y.-X.; Li, Y.; Li, H.; Zhanga, H.-X.; Ren, A.-M. A Theoretical Analysis of the Phosphorescence Efficiencies of Cu(I) Complexes. *Dalton Trans.* **2014**, *43*, 11252−11259.
(36) Bixon, M.; Jortner, J.; Verhoeven, J. W. Lifetimes for Radiative Charge Recombination in Donor-Acceptor Molecules. *J. Am. Chem. Soc.* **1994**, *116*, 7349−7355.
(37) Xie, P.; Chen, Y.-J.; Uddin, M. J.; Endicott, J. F. The Characterization of the High-Frequency Vibronic Contributions to the 77 K Emission Spectra of Ruthenium−Am(m)ine−Bipyridyl Complexes, Their Attenuation with Decreasing Energy Gaps, and the Implications of Strong Electronic Coupling for Inverted-Region Electron Transfer. *J. Phys. Chem. A* **2005**, *109*, 4671−4689.

DOI: 10.1021/jp510949x
J. Phys. Chem. B 2015, 119, 7393−7406

(38) Chen, Y.-J.; Xie, P.; Heeg, M. J.; Endicott, J. F. Influence of the "Innocent" Ligands on the MLCT Excited-State Behavior of Mono(bipyridine)ruthenium(II) Complexes: A Comparison of X-ray Structures and 77 K Luminescence Properties. *Inorg. Chem.* **2006**, *45*, 6282−6297.
(39) Odongo, O. S.; Heeg, M. J.; Chen, Y.-J.; Xie, P.; Endicott, J. F. Effects of Excited State−Excited State Configurational Mixing on Emission Bandshape Variations in Ruthenium−Bipyridine Complexes. *Inorg. Chem.* **2008**, *47*, 7493−7511.
(40) Huckel, W.; Bretschneider, H. *N*-Tripyrazolyl-methan. *Ber. Chem.* **1937**, *70B*, 2024−2026.
(41) Reger, D. L.; Grattan, T. C.; Brown, K. J.; Little, C. A.; Lamba, J. J. S.; Rheingold, A. L.; Sommer, R. D. Syntheses of Tris(pyrazolyl)-methane Ligands and $\{[\text{tris(pyrazolyl)methane}]Mn(CO)_3\}SO_3CF_3$ Complexes: Comparison of Ligand Donor Properties. *J. Organomet. Chem.* **2000**, *607*, 120−128.
(42) Barefied, E. K.; Wagner, F.; Herlinger, A. W.; Dahl, A. R.; Holt, S. (1,4,8,11-Tetraazacyclotetradecane)Nickel(II) Perchlorate and 1,4,8,11-Tetraazacyclotetradecane. *Inorg. Synth.* **1976**, *16*, 220−225.
(43) Chang, J. P.; Fung, E. Y.; Curtis, J. C. Evidence for Specific Solvent-Solute Interactions as a Major Contributor to the Franck−Condon Energy in Intervalence-Transfer Absorptions of Ruthenium Ammine Complexes. *Inorg. Chem.* **1986**, *25*, 4233−4241.
(44) Wong, C.-Y.; Lai, L.-M.; Chan, S.-C.; Tai, L.-H. Photophysical and Theoretical Studies of Ruthenium(II)−Acetylide and −Cyanide Complexes with Aromatic Diimine and Trithiacyclononane. *Organometallics* **2010**, 6259−6266.
(45) Salaymeh, F.; Berhane, S.; Yusof, R.; Rosa, R.; Fung, E. Y.; Matamoros, R.; Lau, K. W.; Zheng, Q.; Kober, E. M.; Curtis, J. C. Electronic Coupling in Mixed-Valence Binuclear Ruthenium Ammine Complexes as Probed by an Electrochemical Method and an Extension of Mulliken's Theory of Donor−Acceptor Interactions. *Inorg. Chem.* **1993**, *32*, 3895−3908.
(46) Bryant, G. M.; Ferguson, J. E.; Powell, H. K. Charge-Transfer and Intraligand Electronic Spectra of Bipyridyl Complexes of Iron, Ruthenium, and Osmium. I. Bivalent Complexes. *Aust. J. Chem.* **1971**, *24*, 257−273.
(47) Chen, Y.-J.; Odongo, O. S.; McNamara, P. G.; Szacilowski, K. T.; Endicott, J. F. Metal-to-Metal Electron-Transfer Emission in Cyanide-Bridged Chromium−Ruthenium Complexes: Effects of Configurational Mixing Between Ligand Field and Charge Transfer Excited States. *Inorg. Chem.* **2008**, *47*, 10921−10934.
(48) Demas, J. N.; Turner, T. F.; Crosby, G. A. Preparation and Thin-Layer Chromatography of Cis-dicyanobis(2,2′-bipyridine)-ruthenium(II). *Inorg. Chem.* **1969**, *8*, 674−675.
(49) Curtis, J. C.; Sullivan, B. P.; Meyer, T. J. Hydrogen-Bonding-Induced Solvatochromism in the Charge-Transfer Transitions of Ruthenium(II) and Ruthenium(III) Ammine Complexes. *Inorg. Chem.* **1983**, *22*, 224−236.
(50) Llobet, A.; Doppelt, P.; Meyer, T. J. Redox Properties of Aqua Complexes of Ruthenium(II) Containing the Tridentate Ligands 2,2′:6′,2″-terpyridine and Tris(1-pyrazolyl)methane. *Inorg. Chem.* **1988**, *27*, 514−520.
(51) Chen, Y.-J.; Xie, P.; Endicott, J. F. Electron-Transfer Emission Spectra of a Cyanide-Bridged, Cr(III)/Ru(II) Donor−Acceptor Complex: High Frequency (N−H and C⋮N) Vibronic Contributions from Empirical Reorganizational Energy Profiles. *J. Phys. Chem. A* **2004**, *108*, 5041−5049.
(52) Endicott, J. F.; Chen, Y.-J.; Xie, P. Electron-Transfer Spectroscopy: Donor−Acceptor Electronic Coupling, Reorganizational Energies, Reaction Pathways and Dynamics. *Coord. Chem. Rev.* **2005**, *249*, 343−373.
(53) Hupp, J. T.; Williams, R. T. Using Resonance Raman Spectroscopy To Examine Vibrational Barriers to Electron Transfer and Electronic Delocalization. *Acc. Chem. Res.* **2001**, *34*, 808−817.
(54) Maruszewski, K.; Bajdor, K.; Strommen, D. P.; Kincaid, J. R. Position-Dependent Deuteration Effects on the Nonradiative Decay of the 3MLCT State of Tris(bipyridine)ruthenium (II). An Experimental Evaluation of Radiationless Transition Theory. *J. Phys. Chem.* **1995**, *99*, 6286−6293.
(55) Myers, A. B.; Mathies, R. A.; Tannor, D. J.; Heller, E. J. Excited State Geometry Changes from Preresonance Raman Intensities: Isoprene and Hexatriene. *J. Chem. Phys.* **1982**, *77*, 3857−3866.
(56) Myers, A. B. Relating Absorption, Emission, and Resonance Raman Spectra with Electron Transfer Rates in Photoinduced Charge Transfer Systems: Promises and Pitfalls. *Chem. Phys.* **1994**, *180*, 215−230.
(57) Myers, A. B. Resonance Raman Intensity Analysis of Excited-State Dynamics. *Acc. Chem. Res.* **1997**, *30*, 519−527.
(58) Thompson, D. G.; Schoonover, J. R.; Timpson, C. J.; Meyer, T. J. Time-Dependent Raman Analysis of Metal-to-Ligand Charge Transfer Excited States: Application to Radiative and Nonradiative Decay. *J. Phys. Chem. A* **2003**, *107*, 10250−10260.
(59) Yersin, H.; Braun, D.; Hensler, G.; Galhuber, E. In *Vibronic Processes in Inorganic Chemistry*; Flint, C. D., Ed.; Kluwer: Dordrecht, The Netherlands, 1989; p 195.
(60) Bloino, J.; Biczysko, M.; Crescenzi, O.; Barone, V. Integrated Computational Approach to Vibrationally Resolved Electronic Spectra: Anisole as A Test Case. *J. Chem. Phys.* **2008**, *128*, 244105−244115.
(61) Santoro, F.; Improta, R.; Lami, A.; Bloino, J.; Barone, V. Effective Method to Compute Franck-Condon Integrals for Optical Spectra of Large Molecules in Solution. *J. Chem. Phys.* **2007**, *126*, 084509−084513.
(62) Santoro, F.; Lami, A.; Improta, R.; Barone, V. Effective Method to Compute Vibrationally Resolved Optical Spectra of Large Molecules at Finite Temperature in the Gas Phase and in Solution. *J. Chem. Phys.* **2007**, *126*, 184102−184111.
(63) Santoro, F.; Lami, A.; Improta, R.; Bloino, J.; Barone, V. Effective Method for the Computation of Optical Spectra of Large Molecules at Finite Temperature Including the Duschinsky and Herzberg−Teller Effect: The Qx Band of Porphyrin as a Case Study. *J. Chem. Phys.* **2008**, *128*, 224311−224317.
(64) Bloino, J.; Biczysko, M.; Santoro, F.; Barone, V. General Approach to Compute Vibrationally Resolved One-Photon Electronic Spectra. *J. Chem. Theory. Comput.* **2010**, *6*, 1256−1274.
(65) Lacky, D. E.; Pankuch, B. J.; Crosby, G. A. Charge-Transfer Excited States of Osmium(II) Complexes. 2. Quantum-Yield and Decay-Time Measurements. *J. Phys. Chem.* **1980**, *84*, 2068−2074.
(66) Demas, J. N.; Crosby, G. A. Quantum Efficiencies on Transition Metal Complexes. II. Charge-Transfer Luminescence. *J. Am. Chem. Soc.* **1971**, *93*, 2841−2847.
(67) Demas, J. N.; Crosby, G. A. Quantum Efficiencies of Transition-Metal Complexes. I. d−d Luminescence. *J. Am. Chem. Soc.* **1970**, *92*, 7262−7270.
(68) Parr, R. G.; Yang, W. *Density-Functional Theory of Atoms and Molecules*; Oxford University Press: New York, 1989.
(69) Frisch, M. J.; Trucks, G. W.; Schlegel, H. B. et al., *Gaussian Development Version*, revision H.20; Gaussian, Inc.: Wallingford, CT, 2010.
(70) Perdew, J. P. Density-Functional Approximation for the Correlation Energy of the Inhomogeneous Electron Gas. *Phys. Rev. B* **1986**, *33*, 8822−8824.
(71) Perdew, J. P.; Burke, K.; Wang, Y. Generalized Gradient Approximation for the Exchange-Correlation Hole of A Many-Electron System. *Phys. Rev.* **1996**, *54*, 16533−16539.
(72) Becke, A. D. Density-Functional Thermochemistry. III. The Role of Exact Exchange. *J. Chem. Phys.* **1993**, *98*, 5648−5652.
(73) Andrae, D.; Haussermann, U.; Dolg, M.; Stoll, H.; Preuss, H. Energy-Adjusted *ab Initio* Pseudopotentials for the Second and Third Row Transition Elements. *Theor. Chim. Acta* **1990**, *77*, 123−141.
(74) Francl, M. M.; Petro, W. J.; Hehre, W. J.; Binkley, J. S.; Gordon, M. S.; DeFrees, D. J.; Pople, J. A. Self-Consistent Molecular Orbital Methods. XXIII. A Polarization-Type Basis Set for Second-Row Elements. *J. Chem. Phys.* **1982**, *77*, 3654−3665.

DOI: 10.1021/jp510949x
J. Phys. Chem. B 2015, 119, 7393−7406

(75) Hariharan, P. C.; Pople, J. A. The Influence of Polarization Functions on Molecular Orbital Hydrogenation Energies. *Theor. Chim. Acta* **1973**, *28*, 213−222.
(76) Bauernschmitt, R.; Ahlrichs, R. Stability Analysis for Solutions of the Closed Shell Kohn−Sham Equation. *J. Chem. Phys.* **1996**, *104*, 9047−9052.
(77) Seeger, R.; Pople, J. A. Self-Consistent Molecular Orbital Methods. XVIII. Constraints and Stability in Hartree−Fock Theory. *J. Chem. Phys.* **1977**, *66*, 3045−3050.
(78) Schlegel, H. B.; McDouall, J. J. In *Computational Advances in Organic Chemistry*; Ögretir, C., Csizmadia, I. G., Eds.; Kluwer Academic: Amsterdam, The Netherlands, 1991.
(79) Marenich, A. V.; Cramer, C. J.; Truhlar, D. G. Universal Solvation Model Based on Solute Electron Density and on a Continuum Model of the Solvent Defined by the Bulk Dielectric Constant and Atomic Surface Tensions. *J. Phys. Chem. B* **2009**, *113*, 6378−6396.
(80) Pennington, R.; Keith, T.; Millam, J. M.; Semichem, Inc.: Shawnee Mission, KS, 2009.
(81) See Supporting Information.
(82) Bersuker, I. B. *The Jahn-Teller Effect and Vibronic Interactions in Modern Chemistry*; Plenum: New York, 1984.
(83) Tsukerblat, B. S. *Group Theory in Chemistry and Spectroscopy*; Academic: London, 1994.
(84) As noted by a reviewer.
(85) Demas, J. N.; Taylor, D. G. On the "Intersystem Crossing" Yields in Ruthenium(II) and Osmium(II) Photosensitizers. *Inorg. Chem.* **1979**, *18*, 3177−3179.
(86) Escudero, D.; Thiel, W. Exploring the Triplet Excited State Potential Energy Surfaces of a Cyclometalated Pt(II) Complex: Is There Non-Kasha Emissive Behavior? *Inorg. Chem.* **2014**, *53*, 11015−11019.
(87) Nozaki, K.; Takamori, K.; Nakatsugawa, Y.; Ohno, T. Theoretical Studies of Phosphorescence Spectra of Tris(2,2′-bipyridine) Transition Metal Compounds. *Inorg. Chem.* **2006**, *45*, 6161−6178.

DOI: 10.1021/jp510949x
J. Phys. Chem. B 2015, 119, 7393−7406